Report on a problem studied at the UK Mathematics-in-Medicine Study Group Nottingham 2002
< http://www.maths-in-medicine.org/uk/2002/dna-condensation/ >

1 The impact of substrate on the measurement of DNA complex morphology

Giles W Richardson & Jonathan AD Wattis,
Theoretical Mechanics Section, School of Mathematical Sciences,
University of Nottingham, University Park, Nottingham, NG7 2RD, U.K.

1.1 Introduction

1.1.1 Outline of problem

In vivo, DNA molecules rarely exist on their own and are normally complexed with a range of molecules ranging from small inorganic molecules to large proteins. The formed complexes and molecular condensates are integral to many cellular processes including DNA replication and molecular compaction within the nucleosome. For this reason much recent attention has focussed upon microscopic techniques that are able to investigate the structure of such complexes. To this end the LBSA in Pharmaceutical Sciences at Nottingham has utilized the atomic force microscope (AFM) to investigate the morphology of a range of DNA molecular complexes including complexes with small intercalating dye molecules, proteins and with polymers intended for gene therapy applications, which cause condensation into rod-shaped and toroidal morphologies (typical images from such experiments are given in, for example, Pope *et al.* [13]).

Implicit to many of the microscopic techniques required to visualise these molecules is theor deposition or immobilization onto a flat surface. The impact of the surface upon the morphology of the condensate, however, remains poorly understood. The study group was thus asked to develop mathematical models to answer the questions:

> (1) Do the structures of the molecules visualised on the surface reflect those in solution?
> (2) For a given population of DNA molecular complexes (with a range of charges/charge densities) is there any preferential adsorption of a particular species onto a defined surface?

1.1.2 Structure of report

After describing the physical set-up of an AFM cell and giving the relevant parameters in the remainder of this section, Section 1.2 of the report describes simple ODE models which aim to answer the former of these two questions. These models are described and solved. Section 1.3 describes in more detail the forces acting in the system and gives a mathematical description of their form. A complete model of the system is then given in Section 1.4. This is given in terms of a system of PDEs by which we aim to answer both the above questions, however, it was not possible to solve this model during the week. Some preliminary results from these models are discussed; finally, in Section 1.5, conclusions are discussed and suggestions for further work are made.

1.1.3 The AFM cell

The AFM cell is a rectangular box, whose base is an approximately 1cm square piece of mica which provides a flat base from which measurements can be made. To perform

experiments in an aqueous environment the cell is filled with a solution of polymer and DNA to a depth of about 1mm. The AFM tip is raised and lowered onto the surface at a rate of 10kHz, and the height of the tip is measured by reflecting a laser beam from the top of the tip. The horizontal resolution of the device is limited by the width of the tip, which can be as little as 2 nm (if a carbon nanotubule tip is used). The vertical resolution is much finer, and fractions of an Ångstrom can be detected. The tip hits the surface with considerable force, and so will deform the structures imaged. A typical experimental configuration is shown in Figure 1.

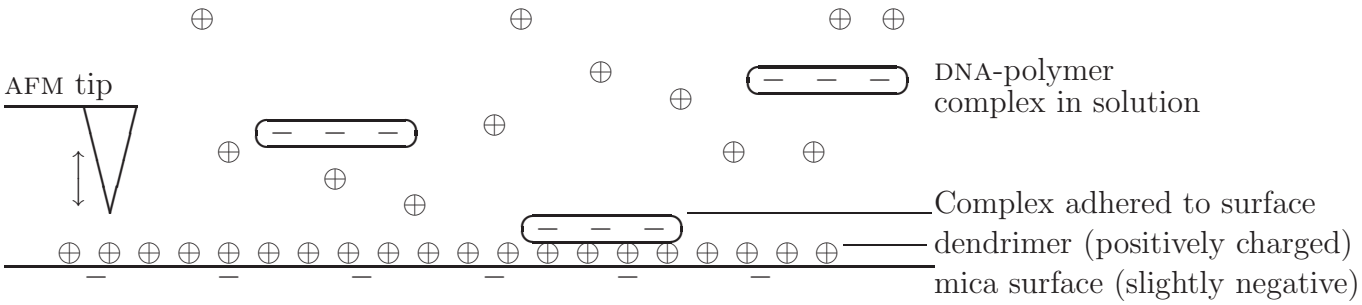

Figure 1: Illustration of the contents of the AFM cell being modelled.

1.1.4 Parameters

Mica surface

Surface charge = 0.015 e^- nm^{-2} = 0.024 C m^{-2}, dielectric constant $\varepsilon_r = 7$.

Dendrimer/Starburst polymer

In solution, the dendrimer is spherical with:

charge: 64 e^- = 10^{-17} C
radius: 2.25 nm = 2.25 $\times 10^{-9}$ m
mass: 2.3×10^{-23} kg
volume: 48 nm^3 = 4.8 $\times 10^{-26}$ m^3
density: 400 kg m^{-3}.

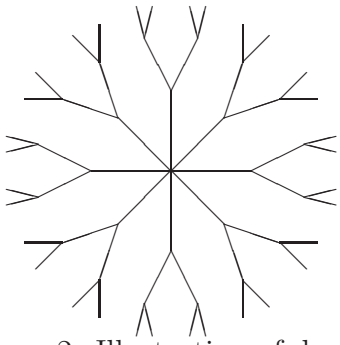

Figure 2: Illustration of dendrimer.

The dendrimer has the form of a 'starburst' polymer – a massively branched polymer, as shown in Figure 2; the charges are located at the outer ends of its branches. The concentration of dendrimers used is typically 2.1μg/ml, this gives a number density of 10^{20} m^{-3} or 100μm^{-3}. Since the volume of the AFM cell is 10^{-7} m^3, the total number of molecules in the cell will be approximately 10^{13}. When adsorbed to the mica surface: the dendrimer alters its shape to that of a hemispherical cap, 15nm in diameter, 0.5 nm high (giving a volume of 44 nm^3, i.e. virtually no change in volume when adhered to the surface).

The surface area covered by each molecule on the surface is 150×10^{-18} m^2; given that the AFM cell is 1cm $\times$ 1cm (10^{-4} m^2), the total number of molecules adhered to the surface is 10^{12}. The covering of the surface by such polymers is analysed by Li *et al.* [11]

and He *et al.* [7] who show the striped and hexagonal patterns which occur due to the high concentration on the surface.

DNA

In solution, open loops of DNA have the form of a cylinder with

radius: 1.15 nm
length: 1455 nm (length of 4300 bps (basepairs))
mass: 5.15 $\times 10^{-21}$ kg
volume: 6050 nm^3 = 6.05 $\times 10^{-24}$ m^3
density: 850 kg m^{-3}
charge: 8600 e$^-$.

The concentration of DNA used is typically 3.3μg/ml. Since each base has a mass of 0.5×10^{-24} kg and there are 8600 bases to each molecule, this concentration corresponds to a number density of 0.77×10^{18} m^{-3} = 0.77μm^{-3}. Since the volume of the cell is 10^{-7} m^3, this corresponds to 0.7×10^{11} molecules.

In each 1 μm^3 there are 64×100=6400 positive charges due to the dendrimer and 0.77×8600= 6622 negative charges, so we have approximate charge neutrality in the system. Bloomfield [1, 2] notes that DNA condensation occurs once approximately 80-90% of the charge is neutralised. However, there are circumstances when charge neutralisations greater than 100% can occur, this is known as charge inversion and has been studied by Nguyen & Shklovskii [12] and Grosberg *et al.* [6].

Note on the effect of gravity

Compared to thermal fluctuations of $kT = 4$ pN nm = 4 $\times 10^{-21}$ J, the energy required to move the DNA 0.5 mm from the centre of the droplet to the surface is $mgd = 2.5 \times 10^{-23}$ J = $\frac{1}{160}kT$, so gravity can safely be ignored. (Even if it were relevant, since the density of the dendrimer and the DNA is less than that of water, buoyancy would cause the complexes to rise and not fall towards the mica surface.)

1.2 Lumped models

1.2.1 Reversible models

We consider two configurations of DNA, type A and type B, we also assume that there are processes which convert A to B and vice versa, and mechanisms by which the DNA can adhere to the surface, and be removed. The states A and B to denote different morphologies of the DNA-polymer complex. In the case of DNA condensation these correspond to rods and toroids; in the case of intercalcators they correspond to the plectonemic, or twisted, rod-like state (either massively undercoiled or massively overcoiled), the other state being the open relaxed case, which, for later calculations, we consider to be effectively a toroidal structure. We assume that the rates for the conversion of A to B and B to A on the substrate and in solution are linear in the concentrations, and similarly for the rates of adhesion to and removal from the substrate. Then the system is as illustrated in Figure 3.

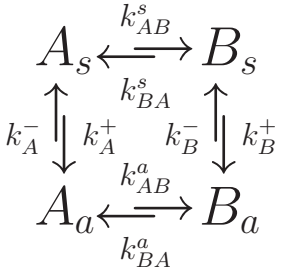

Figure 3: Lumped model of two states of DNA, with each either in solution or adhered to surface.

The kinetic equations are then

$$\begin{aligned}
\dot{A}_s &= k^s_{BA}B_s - k^s_{AB}A_s - k^+_A A_s + k^-_A A_a && (1.1)\\
\dot{B}_s &= k^s_{AB}A_s - k^s_{BA}B_s - k^+_B B_s + k^-_B B_a && (1.2)\\
\dot{A}_a &= k^a_{BA}B_a - k^a_{AB}A_a + k^+_A A_s - k^-_A A_a && (1.3)\\
\dot{B}_a &= k^a_{AB}A_a - k^a_{BA}B_a + k^+_B B_s - k^-_B B_a. && (1.4)
\end{aligned}$$

At equilibrium

$$\frac{B_s}{A_s} = \frac{k^s_{AB}}{k^s_{BA}}, \qquad \frac{B_a}{A_a} = \frac{k^a_{AB}}{k^a_{BA}}, \qquad \frac{A_s}{A_a} = \frac{k^-_A}{k^+_A}, \qquad \frac{B_s}{B_a} = \frac{k^-_B}{k^+_B}. \tag{1.5}$$

So the ratio of type B to type A in solution is given by

$$\frac{k^s_{AB}}{k^s_{BA}} = \frac{B_s}{A_s} = \frac{B_s}{B_a}\frac{B_a}{A_a}\frac{A_a}{A_s} = \frac{k^-_B}{k^+_B}\frac{k^a_{AB}}{k^a_{BA}}\frac{k^+_A}{k^-_A}. \tag{1.6}$$

In the case of DNA condensation, we assume that the number of charges on the rods and toroids are the same, since either one can convert to the other form. Also we assume that the release rates k^-_A and k^-_B are the same since these only depend on the number of bonds to be broken. In this case the (1.6) simplifies to

$$\frac{B_s}{A_s} = \frac{B_a}{A_a}\frac{k^+_A}{k^+_B}. \tag{1.7}$$

The first ratio on the RHS can be measured from AFM experiments, the second can be estimated by the methods described at the end of Section 1.3.

1.2.2 Experimental determination of constants

We denote the total number of complexes of either form and whether attached or in solution by

$$N = A_a + B_a + A_s + B_s. \tag{1.8}$$

At equilibrium, using (1.5), we can rewrite this as

$$1 = \frac{A_a}{N}\left(1 + \frac{k^-_A}{k^+_A}\right) + \frac{B_a}{N}\left(1 + \frac{k^-_B}{k^+_B}\right). \tag{1.9}$$

So plotting B_a/N against A_a/N will give a straight line with intercepts $B_a/N = 1/(1 + k^-_B/k^+_B)$ where $A_a/N = 0$, and $A_a/N = 1/(1 + k^-_A/k^+_A)$ where $B_a/N = 0$, and thus has gradient $(1 + k^-_A/k^+_A)/(1 + k^-_B/k^+_B))$.

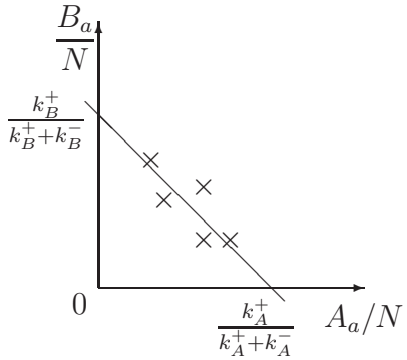

Figure 4: Plotting of experimental data in a way to retrieve the parameters k_A^-/k_A^+ and k_B^-/k_b^+.

1.2.3 Irreversible binding of DNA

In this section we simplify the dynamics of Figure 3, whilst considering the kinetics of the system prior to equilibrium. It is thought that the deposition/removal of material onto and from the surface equilibrates over a timescale longer than 10 minutes, and so measurements are taken before equilibrium is reached. In particular, virtually no removal of complexes from the surface are observed, so we set $k_A^- = 0 = k_B^-$, and simplify the notation by writng $k_A = k_A^+$, $k_B = k_B^+$.

$$\begin{array}{ccc} A_s & \underset{k_{BA}^s}{\overset{k_{AB}^s}{\rightleftharpoons}} & B_s \\ {\scriptstyle k_A}\downarrow & & \downarrow{\scriptstyle k_B} \\ A_a & \underset{k_{BA}^a}{\overset{k_{AB}^a}{\rightleftharpoons}} & B_a \end{array}$$

Figure 5: Lumped model of two states of DNA, with each either in solution or adhered to surface.

Instead of working with the four variables A_s, A_a, B_s, B_a we shall use conservation of the total number of complexes to reduce the system to just three variables

$$X = \frac{A_a}{N}, \qquad Y = \frac{B_a}{N}, \qquad Z = \frac{A_s}{N}, \tag{1.10}$$

with $B_s = N(1 - X - Y - Z)$. Note that X and Y can be observed experimentally, whilst Z cannot. The system of equations can then be written

$$\begin{pmatrix} \dot{X} \\ \dot{Y} \\ \dot{Z} \end{pmatrix} = \begin{pmatrix} -k_{AB}^a & k_{BA}^a & k_A \\ k_{AB}^a - k_B & -k_{BA}^a - k_B & -k_B \\ -k_{BA}^s & -k_{BA}^s & -k_{AB}^s - k_{BA}^s - k_A \end{pmatrix} \begin{pmatrix} X \\ Y \\ Z \end{pmatrix} + \begin{pmatrix} 0 \\ k_B \\ k_{BA}^s \end{pmatrix}. \tag{1.11}$$

This system can be solved by

$$\begin{pmatrix} X \\ Y \\ Z \end{pmatrix} = \sum_{i=1}^{3} C_i e^{\theta_i t} \mathbf{v}_i + \begin{pmatrix} X_\infty \\ Y_\infty \\ 0 \end{pmatrix}, \tag{1.12}$$

where the eigenvalues θ_i are all negative and are given by

$$\theta_1 = -k^a_{AB} - k^a_{BA}, \qquad \theta_{2,3} = \frac{-1}{2}\left(k_B + k_A + k^s_{AB} + k^s_{BA} \pm \sqrt{(k_A - k_B + k^s_{AB} - k^s_{BA})^2 + 4k^s_{AB}k^s_{BA}}\right), \tag{1.13}$$

and the vectors $\mathbf{v}_i$ are the corresponding eigenvectors. At $t = 0$ there is no material on the surface, so the constants C_i will be determined by $X(0) = 0 = Y(0)$ and one further condition which indicates the number of type A condensates in solution at small times.

The challenge is then to find the six rate parameters $(k_A, k_B, k^s_{AB}, k^s_{BA}, k^a_{AB}, k^a_{BA})$ by observing the evolution of $X(t)$ and $Y(t)$ over time and fitting their evolution to the solution (1.12).

1.3 Forces involved in surface attraction

We now give the form of the forces acting on the DNA and polymers which may be responsible for their landing on the surface. Other than the electrostatic force, there are van der Waals forces, and hydrophobic forces which attract particles from the bulk to the surface, and viscous drag which slows any resultant motion and consequently hinders the deposition of material on the surface.

1.3.1 Hydrophobic

The energy associated with hydrophobic interactions can be modelled by $E_{\text{hydro}} = -2\gamma e^{-x/\lambda}$ with $\lambda = 1 - 2$ nm, $\gamma = 10 - 50 \times 10^{-3}$ J m^{-2}, and x being the separation of the particle from the surface [9]. For a dendrimer in solution, with a surface area of 64 nm^2, the energy in the hydrophobic interaction exceeds kT in a region extending only 7nm away from the mica surface.

1.3.2 Van der Waals forces

We continue to use x to denote the distance between the surfaces: for a surface-point charge the energy of interaction is given by $E_{\text{VdW}} = -C\pi p/6x^3$; [9] for a sphere-surface interaction by

$$E_{\text{VdW}} = -\frac{AR}{6x}, \tag{1.14}$$

where R is the radius of the sphere, and A is the Hamaker constant. For the interaction between two parallel cylinders $E_{\text{VdW}} = AL\left(\frac{R_1R_2}{R_1+R_2}\right)^{1/2}/12\sqrt{2}x^{3/2}$,
which in the limit of large radius for one of the cylinders gives $E_{\text{VdW}} = AL\sqrt{R}/12\sqrt{2}x^{3/2}$. Here, L is treated as the length of the cylinder, and R its radius, the other cylinder becoming the plane in the limit $R \to \infty$.

The Hamaker constants $A_{\text{mica-water-mica}} = 2 \times 10^{-20}$J and $A_{\text{Al-water-Al}} = 5 \times 10^{-20}$J can be combined to find $A_{\text{mica-water-Al}} = \sqrt{A_{\text{mica-water-mica}}A_{\text{Al-water-Al}}} = 3 \times 10^{-20}$ J. Taking the dendrimer to be a sphere and using (1.14) the energy of this interaction exceeds kT only within 3nm of the surface. For a piece of DNA 1500 nm long and with a radius of 1 nm, the energy of the van der Waals interaction exceeds kT for all of the 76 nm closest to the mica surface.

1.3.3 Viscous drag

The drag on a particle in a viscous fluid is dependent on its shape, with the well-known result $F_{\text{drag}} = 6\pi\mu aU$ for spheres. In this report, however, we are concerned with a variety of other shapes, we quote results here for the rod and the toroid.

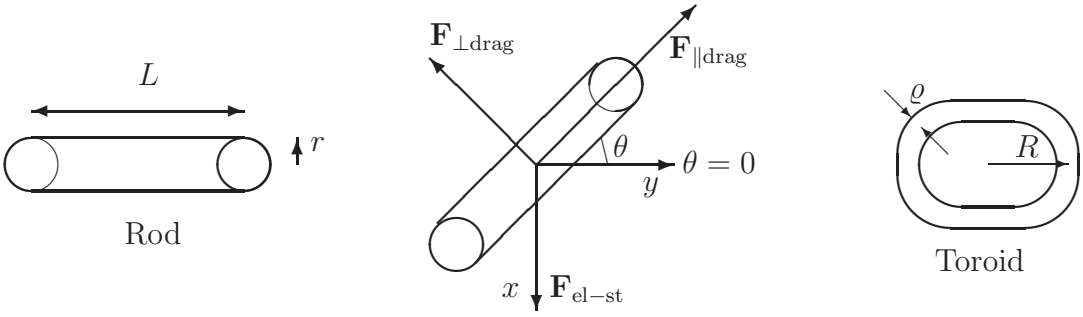

Figure 6: Notation used in describing rods and toroids.

The motion of slender objects falling through a viscous fluid has been analysed in the literature and the formulae for the associated drag forces are as below. A long cylindrical rod falls through a viscous fluid faster along its major axis than its minor axis with the associated speed-force relationships being

$$F_{\parallel\text{rod}} = \frac{-2\pi\mu L U_\parallel}{\log(L/r) - 0.72}, \qquad F_{\perp\text{rod}} = \frac{-4\pi\mu L U_\perp}{\log(L/r) - C_\perp}. \tag{1.15}$$

See Cox [3, 4] for details of the derivation of this formula. In a similar manner, slender toroids fall faster in their plane (denoted by the subscript $\parallel$) than perpendicular to it (subscript $\perp$), with the viscous drag in these directions being given by

$$F_{\parallel\text{toroid}} = \frac{-6\pi^2\mu R U_\parallel(\log(8R/\varrho) - 17/6)}{(\log(8R/\varrho) - 2)(\log(8R/\varrho) - 1/2) - 2}, \qquad F_{\perp\text{toroid}} = \frac{-8\pi^2\mu R U_\perp}{\log(8R/\varrho) + 1/2}. \tag{1.16}$$

See Johnson & Wu [10] for further details. For simplicity we now only retain the leading order terms for large L/r or R/ϱ. An alternative way of thinking about the above formulae is to define an effective, or 'Stokes' radius' denoted by a for a particle for which the formula $F = -6\pi\mu aU$ can then be used. With this definition we have $a = L/3\log(L/r)$ for the rod and $a = \pi R/\log(R/\varrho)$ for the toroid.

Resolving forces in the above diagram (Figure 6) we find

$$F_\parallel = -F_{\text{el-st}}\sin\theta, \qquad F_\perp = -F_{\text{el-st}}\cos\theta, \tag{1.17}$$

so that for the rod, (1.15) implies

$$U_{\parallel\text{rod}} = \frac{F_{\text{el-st}}\sin\theta\log(L/r)}{2\pi\mu L}, \qquad U_{\perp\text{rod}} = \frac{F_{\text{el-st}}\cos\theta\log(L/r)}{4\pi\mu L}. \tag{1.18}$$

The vertical and horizontal velocities are then given by

$$U_x = U_\parallel\sin\theta + U_\perp\cos\theta, \qquad U_y = U_\parallel\cos\theta - U_\perp\sin\theta, \tag{1.19}$$

so that

$$U_{x,\text{rod}} = \frac{F_{\text{el-st}}(1+\sin^2\theta)\log(L/r)}{4\pi\mu L}, \qquad U_{y,\text{rod}} = \frac{F_{\text{el-st}}\sin\theta\cos\theta\log(L/r)}{4\pi\mu L}. \tag{1.20}$$

The total speed, and direction of the descent is given by

$$U_{\rm rod} = \frac{F_{\rm el-st}\log(L/r)\sqrt{1+3\sin^2\theta}}{4\pi\mu L}, \qquad \tan\psi_{\rm rod} = \frac{\sin\theta\cos\theta}{1+\sin^2\theta}. \tag{1.21}$$

For the toroidal configuration, similar calculations using (1.16), (1.17) and (1.19) lead to

$$U_{x,\rm toroid} = \frac{F_{\rm el-st}(3+\sin^2\theta)\log(8R/\varrho)}{24\pi^2\mu R}, \qquad U_{y,\rm toroid} = \frac{F_{\rm el-st}\sin\theta\cos\theta\log(8R/\varrho)}{24\pi^2\mu R}. \tag{1.22}$$

The total speed, and direction of the descent of a toroid is given by

$$U_{\rm toroid} = \frac{F_{\rm el-st}\log(8R/\varrho)\sqrt{9+2\sin^2\theta}}{24\pi^2\mu R}, \qquad \tan\psi_{\rm toroid} = \frac{\sin\theta\cos\theta}{3+\sin^2\theta}. \tag{1.23}$$

The volume of a rod with radius r and length L is $\pi r^2 L$, and since we are assuming narrow rods, (i.e. small aspect ratio r/L), we can define its length as L. The volume of a torus with major and minor radii R, ϱ respectively, is $V = 2\pi R\varrho^2$, and length $2\pi R$, assuming $\varrho \ll R$. In the process of conversion from one to the other, we assume that the volume remains the same. So as to have definite formulae linking (r, L) with (R, ϱ) we shall also assume that the length remains the same, thus we find

$$L = 2\pi R, \qquad r = \varrho/\sqrt{\pi}. \tag{1.24}$$

To leading order in the aspect ratio ($r/L \ll 1$), the velocity of a falling rod is given by (1.20), whereas the converting the velocity of a toroid from R, ϱ variables to L, r using (1.24) yields

$$U_{x,\rm toroid} = \frac{F_{\rm el-st}(1+\frac{1}{3}\sin^2\theta)\log(L/r)}{4\pi\mu L}. \tag{1.25}$$

For $\theta \neq 0$, we see that $U_{\rm rod} \geq U_{\rm toroid}$, so that for a given force, the rod falls faster than the toroid. At $\theta = 0$, which is the slowest orientation of descent, rods and toroids fall at the same speed. For other angles the ratios of the rates of descent $U_{x,\rm rod}/U_{x,\rm toroid}$ varies between 1 and 1.5. Thus complexes fall slightly faster in the rod structure than in the toroidal form, so if there were a region in the bulk, near the surface where the timescale for equilibration between rods and toroids were slower than the rate of deposition then one would expect rods to be overexpressed on the surface. However, if rods and toroids are in equillibrium with each other at all distances from the mica surface, then they will be in equilibrium on the surface too, and the ratio of observed structures on the surdace will be a fair representation of that in the bulk solution.

Formally averaging the expressions for U_x in (1.20) and (1.25) over all possible directions (a solid angle of 4π steradians in three-dimensional space) by the formula

$$\langle f(\theta,\phi)\rangle = \frac{1}{4\pi}\int_{\theta=0}^{\pi}\int_{\phi=0}^{2\pi} f(\theta,\phi)\sin\theta\, d\theta\, d\phi, \tag{1.26}$$

we find

$$\langle U_{x,\rm rod}\rangle = \frac{5F_{\rm el-st}\log(L/r)}{12\pi\mu L}, \qquad \langle U_{x,\rm toroid}\rangle = \frac{11F_{\rm el-st}\log(8R/\varrho)}{72\pi^2\mu R} = \frac{11F_{\rm el-st}\log(L/r)}{36\pi\mu L}. \tag{1.27}$$

Thus it appears that on average rods will be over-expressed on the surface by a factor of 15/11.

The rate of deposition on the surface can be found by balancing the attractive forces (van der Waals, hydrophobic, electrostatic) with the viscous drag. Thus we can find a characteristic velocity for each shape of particle deposited on the surface. A model which incorporates all these forces is described in the next section.

1.4 A model for dendrimer and DNA adhesion to a plate

In this section we consider a detailed model for dendrimer and DNA adhesion to a charged plate. In its un-neutralised state DNA is negatively charged and forms long thin chains. The dendrimer is a positively charged ball like molecule with a valency of 64. When it is added to a solution of DNA it combines with the negatively charged DNA. When enough dendrimer has combined with a strand of DNA to neutralise about 90/100 of its charge the DNA coils up (condenses) to form one of two possible complexes; that is either a supercoiled torus or a supercoiled rod-like structure (or plectoneme). In the experiments we are asked to consider, dendrimer is added to the DNA and then deposited as a drop onto a mica plate. This plate initially carries a negative charge and, it is hypothesised, that this acts to attract the positively charged polymer to its surface. The polymer then binds to the surface through the action of short range forces (the van der Waals force and the hydrophobic force). In experiments a rather surprising observation is made, namely that the amount of polymer which binds to the surface neutralises its nett negative charge many times over leaving the surface positively charged. The now positively charged plate acts to attract the large (and negatively charged) DNA complexes. These again bind to the surface through short range interactions and may be observed using an atomic force microscope. Our aim here is to develop a model for these processes with the eventual goal of finding out whether a different ratio of the two DNA species is found in solution from that found on the surface and if so how these two quantities can be related.

We make use of the small aspect ratio of the experimental set-up (the ratio of distances between points in the solution and the mica surface to the width of the surface are small) to make a one-dimensional model for migration of particles (polymer and DNA) through the solution to the surface and their adhesion (see figure 7). The variables we use in the model are

x : distance form the mica plate,
c_r : concentration of rods in solution,
c_o : concentration of toroids in solution,
c_d : concentration of dendrimer in solution,
v_r : velocity of rods in absence of diffusion,
v_o : velocity of toroids in absence of diffusion,
v_d : velocity of dendrimer in absence of diffusion,
Γ_r : surface concentration of rods,
Γ_o : surface concentration of toroids,
Γ_d : surface concentration of dendrimer,
$\boldsymbol{E}$: the electric field,

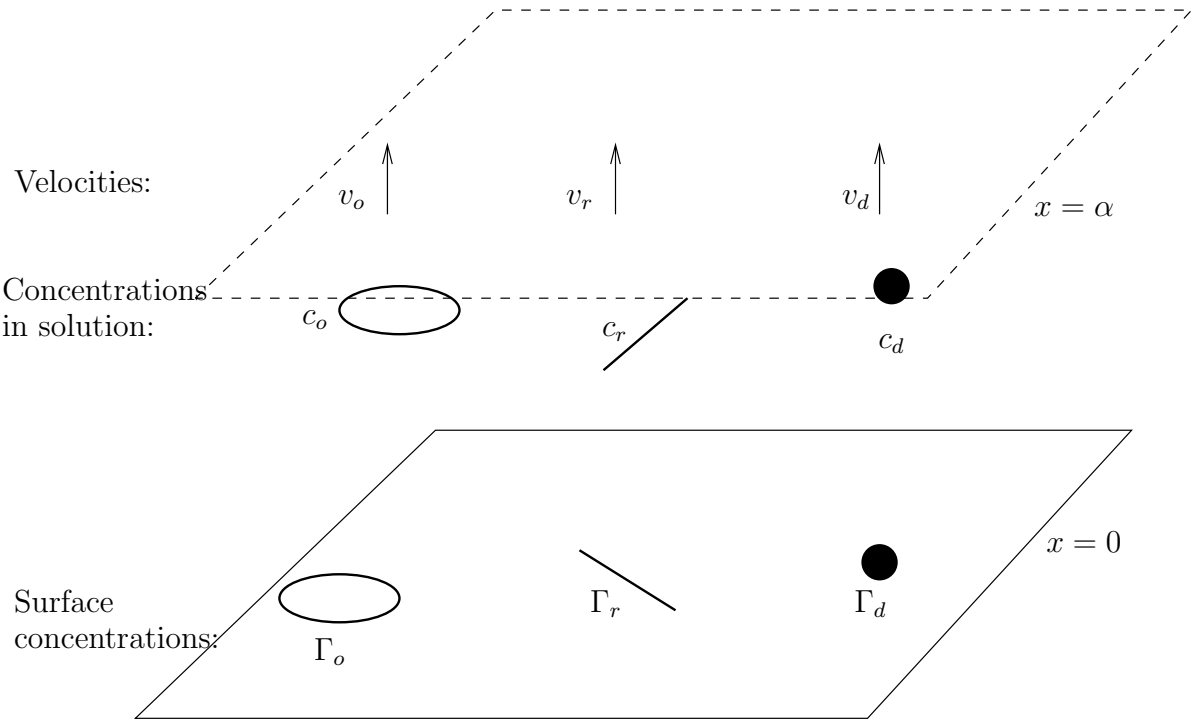

Figure 7: A schematic of the model

In addition we make use of the following parameters

D_r :	diffusivity of rods,
D_o :	diffusivity of toroids,
D_d :	diffusivity of dendrimer,
a_r :	the Stokes' radius of a rod,
a_o :	the Stokes' radius of a toroid,
a_d :	the Stokes' radius of a dendrimer,
q_r :	the electric charge on a rod,
q_o :	the electric charge on a toroid,
q_d :	the electric charge on a dendrimer,
μ :	the viscosity of water,
k :	Boltzmann's constant,
α :	the height of the solution surface above the mica plate,
T :	the absolute temperature.

The particles (rods, toroids and dendrimer) are all acted upon by electrostatic force, Stokes drag, the Van der Waals' force and the hydrophobic force. The last two of these are short range force which only act over the range of several nanometres from the surface. Since the drop of solution applied to the mica surface has thickness many thousands of times bigger than these lengthscales and since both forces are poorly understood our approach will be to (i) model the transport of particles in solution using only the Stokes drag and the electrostatic forces and (ii) incorporate the effects of Van der Waals' forces and hydrophobic forces into the Gibbs Free energy of the surface (this is standard practice).

The velocity $\boldsymbol{v}$ of a single species of particle with charge q, in the absence of thermal fluctuations, which moves in a dilute solution under the action of an electrostatic field $\boldsymbol{E}$

is found by equating the Stokes drag with the electrostatic force; this gives

$$6\pi\mu a\boldsymbol{v} = q\boldsymbol{E},$$

where a is the Stokes radius of the particle (*i.e.* its radius if it is spherical). In reality small particles may experience significant random fluctuations in their velocity due to thermal fluctuations (Brownian motion). When averaged over a large number of particles this random motion gives rise to a diffusive part to the motion whose coefficient of diffusion D can be found using the Einstein relation

$$D = \frac{kT}{6\pi\mu a}.$$

In one dimension, with $\boldsymbol{v} = v\boldsymbol{e_x}$ and $\boldsymbol{E} = E\boldsymbol{e_x}$, conservation of particles is expressed by the following partial differential equation

$$\frac{\partial c}{\partial t} + \frac{\partial}{\partial x}(\boldsymbol{v}c) = D\frac{\partial^2 c}{\partial x^2}.$$

This is easily generalised to the case where there is more than one species of non-interacting particle in solution. In the instance we consider, there are three species of particle, namely rods, toroids and dendrimer and we would like to allow for the fact that there is a rate of conversion from toroids to rods and back again. The evolution equations for the concentrations of rods, toroids and dendrimer then read

$$\frac{\partial c_r}{\partial t} + \frac{\partial}{\partial x}(c_r v_r) = D_r\frac{\partial^2 c_r}{\partial x^2} - \chi c_r + \nu c_r \tag{1.28}$$

$$\frac{\partial c_o}{\partial t} + \frac{\partial}{\partial x}(c_o v_o) = D_o\frac{\partial^2 c_o}{\partial x^2} + \chi c_r - \nu c_o \tag{1.29}$$

$$\frac{\partial c_d}{\partial t} + \frac{\partial}{\partial x}(c_d v_d) = D_d\frac{\partial^2 c_d}{\partial x^2}. \tag{1.30}$$

Here the coupling term on the right-hand sides of (1.28) and (1.29) represent conservation of the total numbers of rods and dendrimers and an equilibrium ratio of the two concentrations of $c_r/c_o = \nu/\chi$. The fact we allow transfer between rods and toroids without the consumption, or production, of dendrimer means that we implicitly assume $q_r = q_o$, since otherwise charge is not conserved. The diffusion coefficients and the velocities are calculated as before so that, for the i'th species (where $i = r, o, d$)

$$D_i = kT/6\pi\mu a_i, \qquad v_i = q_i E/6\pi\mu a_i. \tag{1.31}$$

The Stokes radii of the spherical dendrimer a_d is just the radius of the dendrimer particle. The Stokes radii of toroids a_o and rods a_r can be derived from calculations of the drag on a toroid and a rod made in Section 1.3.3.

The electric field is found from Maxwell's equations and, although an electric current flows due to the movement of charged particles, we can approximate these by the equations of electrostatics

$$\boldsymbol{E} = \nabla\phi, \qquad \nabla\cdot(\varepsilon\boldsymbol{E}) = \rho, \tag{1.32}$$

because the size of the currents flowing causes only very small changes to the electric field. Here ρ is the charge density and is found by considering the local concentration of

particles and their charges; thus $\rho = c_d q_d + c_0 q_o + c_r q_r$. Substitution of this expression for the charge density back into the equations of electrostatics, in our one-dimensional scenario, leads to the following equations for the electric field

$$\frac{\partial^2 \phi}{\partial x^2} = \frac{c_d q_d + c_o q_o + c_r q_r}{\varepsilon} \quad \text{where} \quad E = \frac{\partial \phi}{\partial x}. \tag{1.33}$$

In formulating (1.33) we have assumed that the nett charge carried by the three species of particle is zero; that is

$$(q_r \Gamma_r + q_o \Gamma_o + q_d \Gamma_d) + \int_0^\alpha (q_r c_r + q_o c_o + q_d c_d) dx = 0, \tag{1.34}$$

where Γ_r, Γ_o and Γ_d are the surface charges of the rods toroids and dendrimer respectively. Where this assumption does not hold we must allow for a further species (*e.g.* hydrogen ions) and consequently write down a further set of conservation equations for the concentration of this new species.

Boundary conditions must now be imposed for the concentrations c_r, c_o and c_d both on the upper surface of the film covering the mica plate $x = \alpha$ and on the the mica surface $x = 0$. On $x = \alpha$ there is zero flux of particles through the boundary so that

$$c_i v_i - D_i \frac{\partial c_i}{\partial x}\bigg|_{x=\alpha} = 0, \qquad (\text{where } i = r, o, d). \tag{1.35}$$

On the mica surface $x = 0$ we require conservation of particles and this enforces the conditions

$$\dot{\Gamma}_i \;=\; D_i \frac{\partial c_i}{\partial x} - c_i v_i\bigg|_{x=0} \qquad (\text{where } i = r, o, d). \tag{1.36}$$

We require a further relation between the surface concentrations Γ_i and the solution's concentrations c_i. This is provided by minimising Gibb's free energy of the surface G with respect to the surface concentrations Γ_i. This is given by the formula

$$\begin{aligned} \frac{G}{kTA} \;=\; & \sum_i \Gamma_i \log(\Gamma_i A) + (\Gamma^* - \sum_i \Gamma_i) \log\left(\Gamma^* A - \sum_i \Gamma_i A\right) \\ & - \sum_i \Gamma_i \left(\frac{\mu_i^*}{kT} + \log(c_i A h)\right) - \frac{\beta\phi}{kT} \sum_i q_i \Gamma_i, \end{aligned} \tag{1.37}$$

where A is the total surface area of the base of the AFM cell, and h is a typical height over which surface interactions occur. Later calculations do not depend on the values of A or h. The sums range over $i = r, o, d$; k is the Boltzmann's constant; μ_i^* the chemical potential of the i'th species; and β is a dimensionless constant prescribing the relative strength of the electrostatic interactions to the packing of the surface. The effect of the large electric fields could be moderated by using small values of this parameter in a similar manner to the tuning of Stern parameter (see (1.40)). Carrying out the minimisation by setting $\delta G / \delta \Gamma_i = 0$ leads to a relation for the surface concentrations in terms of the solutions concentration and the potential evaluated at $x = 0$:

$$\Gamma_j = \frac{\Gamma^* c_j \exp((\mu_j^* + \beta\phi q_j)/kT)}{1 + \sum_i c_i \exp((\mu_i^* + \beta\phi q_i)/kT)}\bigg|_{x=0}. \tag{1.38}$$

In addition we require a boundary condition for the potential ϕ on the surface $x = 0$. This is provided by integrating the electrostatic equation $(\varepsilon E)_x = \rho$ across $x = 0$ and assuming that the electric field vanishes on the other side of the plate. This gives

$$\phi_x|_{x=0} = E|_{x=0} = \frac{1}{\varepsilon}\sum_i q_i\Gamma_i.$$

Finally we require a condition on the potential on $x = \alpha$. Using the condition of no nett charge (1.34) we can show that (1.39) implies $\phi_x|_{x=\alpha} = 0$ and hence that the potential on $x = \alpha$ is the potential at infinity. We thus impose the condition

$$\phi|_{x=\alpha} = 0. \tag{1.39}$$

However in practice this neglects an important part of the physics. The chemical potential of the surface can lead to a significant surface charge which in turn leads to a large electric field at the surface. This causes dissociation of the water molecules just above the surface in a narrow layer in the vicinity of the surface with the many of the negatively charged 'water ions' being attracted to the surface and decreasing its effective charge while the positively charged 'water ions' are free to diffuse about the solution. In order to overcome this difficulty the boundary condition (1.39) is sometimes rewritten in the form

$$\phi_x|_{x=0} = E|_{x=0} = \frac{S_T}{\varepsilon}\sum_i q_i\Gamma_i, \tag{1.40}$$

where here the Stern parameter S_T is a positive constant which is less than one. However, this has the unfortunate consequence that the nett charge in the system is no longer zero and hence that (1.34) is not satisfied. Furthermore we are unaware of data giving the value of S_T, although preliminary calculations suggest that it could be very small ($S_T \sim 10^{-4}$).

Estimates of some of the parameters in the model It is useful to estimate some of the parameters in the model in order to see which terms can be neglected. Estimates of some of the parameters in the model are given below

$$a_r \sim 10^{-7}\ \text{m}, \qquad a_o \sim 10^{-7}\ \text{m}, \qquad a_d \sim 2.5\times 10^{-9}\ \text{m}$$
$$q_r \sim 0 - 1.6\times 10^{-16}\ \text{C}, \qquad q_o \sim 0 - 1.6\times 10^{-16}\ \text{C}, \qquad q_d \sim 10^{-17}\ \text{C}$$
$$\mu \sim 10^{-3}\ \text{kg m}^{-1}\text{s}^{-1}, \qquad k = 1.381\times 10^{-23}\ \text{N m Kelvin}^{-1}, \qquad T \sim 310\,\text{Kelvin}$$
$$\alpha = 10^{-4}\text{m} \qquad \varepsilon = 7.16\times 10^{-8}\text{CV}^{-1}\text{m}^{-1}$$

We may use the above to get estimates of the diffusion coefficients

$$D_r \sim 10^{-10}\text{m}^2\text{s}^{-1}, \quad D_o \sim 10^{-10}\text{m}^2\text{s}^{-1}, \quad D_d \sim 10^{-8}\text{m}^2\text{s}^{-1}.$$

The timescale τ_i for the i'th component to diffuse across the solution layer is

$$\tau_i = \frac{\alpha^2}{D_i}.$$

Thus the typical timescales for diffusion of dendrimer across the solution is 1s and for the DNA is more like 100s. Both these timescales are relatively short compared to the

duration of the experiment and so suggest that we can neglect time derivatives in (1.28)-(1.30), (1.31) and (1.36) and then look at a steady state model. Note however that the timescale is rather sensitive to changes in the thickness of the solution layer α and that it would not take that large an increase in α for τ_r and τ_o to become comparable to, or even larger than, the experimental timescale.

1.5 Conclusions and future work

We have tried to tackle this problem in two different ways. In Section 1.2 we wrote down rate equations for the transfer between the two species of DNA in solution and adhered to the mica substrate. In Section 1.4 we looked at a more detailed model of this process which includes the dynamics and electrostatic interactions of the various species. At first sight this more complicated model seems to reduce to the simple model of section 1.2 in the limit where the exchange reaction between the two species of DNA (rods and polymers) is much faster than the dynamic processes (diffusion and advection). However while this may be true for the bulk of the solution it is not true in a boundary layer close to the mica substrate in which dynamic processes are still important. This provides good motivation for the further study of this more complex model.

Contributors

Stephanie Allen, John Billingham, Chris Breward, Helen Byrne, Jon Chapman, Hosam Gharib-Abdelhody, Deirdre Hollingsworth, Peter Howell, Oliver Jensen, John King, Eugene Maltsev, John Norbury, Colin Please, Giles Richardson, Jonathan Wattis.

References

[1] V Bloomfield. Condensation of DNA by multivalent cations - considerations on mechanism. *Biopolymers*, **31**, 1471–1481, (1991).

[2] V Bloomfield. DNA condensation by multivalent cations. *Biopolymers*, **44**, 269–282, (1997).

[3] RG Cox. Motion of long slender bodies in a viscous fluid-part 1: general theory. *J Fluid Mech*, **44**, 791–810, (1970).

[4] RG Cox. Motion of long slender bodies in a viscous fluid-part 2: shear flow. *J Fluid Mech*, **45**, 625–657, (1971).

[5] BS Fujimoto & JM Schurr. Monte Carlo simulations of supercoiled DNAs confined to a plane. *Biophys J*, **82**, 944-962, (2002).

[6] AY Grosberg, TT Nguyen & BI Shklovskii. Colloquium: the physics of charge inversion in chemical and biological systems. *Rev Mod Phys*, **74**, 329–345, (2002).

[7] X He, L Huang, H Liang & C Pan. Self-assembly of star block copolymers by dynamic density functional theory. *J Chem Phys*, **116**, 10508–10513, (2002).

[8] RJ Hunter. *Zeta Potential in Colloid Science: Principles and Applications*. Academic Press, London, (1981).

[9] J Israelachvili. *Intermolecular and Surface Forces*. Second Edition, Academic Press, London, (1992).

[10] RE Johnson & TY Wu. Hydrodynamics of low Reynolds flow, part 5 motion of a slender torus. *J Fluid Mech*, **95**, 263–277, (1979).

[11] J Li, TT Piehler, D Qin, JR Baker & DA Tomalia. Visualisation and characterisation of poly(amidoamine) dendrimers by atomic force microscopy. *Langmuir* **16**, 5613–5616, (2000).

[12] TT Nguyen & BI Shklovskii. Complexation of DNA with positive spheres: phase diagram of charge inversion and reentrant condensation. *J Chem Phys*, **115**, 7298–7308, (2001).

[13] LH Pope, MC Davies, CA Laughton, CJ Roberts, SJB Tendlar, & PM Williams. Intercalation-induced changes in DNAsupercoiling observed in real time by atomic force microscopy. *Anal Chim Acta*, **400**, 27–32, (1999).